Melissa: Bayesian clustering and imputation of single cell methylomes

Melissa: Bayesian clustering and imputation of single cell methylomes

Chantriolnt-Andreas Kapourani[1,2,*] C.A.Kapourani@ed.ac.uk
Guido Sanguinetti[1,3,*] G.Sanguinetti@ed.ac.uk

[1]School of Informatics, University of Edinburgh, Edinburgh EH8 9AB, UK
[2]MRC Institute of Genetics and Molecular Medicine, University of Edinburgh, Edinburgh EH4 2XU, UK
[3]Synthetic and Systems Biology, University of Edinburgh, Edinburgh EH9 3BF, UK
[*]To whom correspondence should be addressed

Abstract

Measurements of single-cell methylation are revolutionizing our understanding of epigenetic control of gene expression, yet the intrinsic data sparsity limits the scope for quantitative analysis of such data. Here, we introduce Melissa (MEthyLation Inference for Single cell Analysis), a Bayesian hierarchical method to cluster cells based on local methylation patterns, discovering patterns of epigenetic variability between cells. The clustering also acts as an effective regularization for data imputation on unassayed CpG sites, enabling transfer of information between individual cells. We show both on simulated and real data sets that Melissa provides accurate and biologically meaningful clusterings, and state-of-the-art imputation performance.

1 Background

DNA methylation is probably the best studied epigenomic mark, due to its well established heritability and widespread association with diseases and a broad range of biological processes, including X-chromosome inactivation, cell differentiation and cancer progression (Baylin and Jones, 2011; Bird, 2002; Jones, 2012). Yet its role in gene regulation, and the molecular mechanisms underpinning its association with diseases, are still imperfectly understood.

Bisulfite treatment of DNA followed by sequencing (BS-seq) has provided a powerful tool for measuring the methylation level of cytosines on a genome-wide scale with single nucleotide resolution (Krueger *et al.*, 2012). BS-seq protocols have been vastly improved over the last decade, with BS-seq rapidly becoming a widespread tool in biomedical investigation. Nevertheless, until very recently BS-seq could only be used to measure methylation in bulk populations of cells (Shapiro *et al.*, 2013), preventing effective investigations of the role of DNA methylation in shaping transcriptional variability and early development (Kelsey *et al.*, 2017; Schwartzman and Tanay, 2015).

This shortcoming has been addressed within the last five years through the development of protocols to measure DNA methylation at single-cell resolution using either scBS-seq (Smallwood *et al.*, 2014) or scRRBS (Guo *et al.*, 2013) making it possible to uncover the heterogeneity and dynamics of DNA methylation (Farlik *et al.*, 2015). Even more recently, methods have been developed that can sequence both the methylome and the transcriptome or other features in parallel, potentially enabling a quantification of the role of DNA methylation in explaining transcriptional heterogeneity (Angermueller *et al.*, 2016; Clark *et al.*, 2018; Hou *et al.*, 2016). However, due to the small amounts of genomic DNA per cell, these protocols usually result in very sparse genome-wide CpG coverage (i.e. for most CpGs we have missing values), ranging from 5% in high throughput studies (Luo *et al.*, 2017; Mulqueen *et al.*, 2018) to 20% in low throughput ones (Angermueller *et al.*, 2016; Smallwood *et al.*, 2014). The sparsity of the data represents a major hurdle to effectively use single-cell methylation assays to inform our understanding of epigenetic control of transcriptomic variability, or to distinguish individual cells based on their epigenomic state.

In this paper, we address these problems by using a two-pronged strategy. First, we note that several recent studies have highlighted the importance of local methylation profiles, as opposed to individual CpG methylation, in determining the epigenetic state of a region (Kapourani and Sanguinetti, 2016; Mayo *et al.*, 2015; Vanderkraats *et al.*, 2013). This implies that local spatial correlations may be effectively leveraged to ameliorate the issue of data sparsity. Secondly, single-cell BS-seq protocols, as all single-cell high-throughput protocols, simultaneously assay a large number of cells, ranging from several tens (Smallwood *et al.*, 2014) to a few thousands in the most recent studies (Luo *et al.*, 2017). Such abundance of data could be exploited to our advantage to transfer information across similar cells.

We implement both of these strategies within Melissa (MEthyLation Inference for Single cell Analysis), a Bayesian hierarchical model that jointly learns the methylation profiles of genomic regions of interest and clusters cells based on their genome-wide methylation patterns. In this way, Melissa can effectively use both the information of neighbouring CpGs and of other cells with similar methylation patterns in order to predict CpG methylation states. As an additional benefit, Melissa also provides a Bayesian clustering approach capable of identifying subsets of cells based solely on epigenetic state, to our knowledge the first clustering method tailored specifically to this rapidly expanding technology. We benchmark Melissa on both simulated and real single-cell BS-seq data, demonstrating that Melissa provides both state of the art imputation performance, and accurate clustering of cells. Furthermore, thanks to a fast variational Bayes estimation strategy, Melissa has good scalability and can provide an effective modelling tool for the increasingly large single-cell methylation studies which will become prevalent in coming years.

2 Results and discussion

Melissa addresses the data sparsity issue by leveraging local correlations between neighbouring CpGs and similarity between individual cells (see Fig. 1). The starting point is the definition of a set of genomic regions (e.g. genes or enhancers) over which the model will be applied. Within each region, Melissa postulates a latent profile of methylation, a function mapping each CpG within the region to a number in $[0, 1]$ which defines the probability of that CpG being methylated. To ensure spatial smoothness of the profile, Melissa uses a generalised linear model (GLM) of basis function regression along the lines of Kapourani and Sanguinetti (2016) (with modified likelihood to account for single cell data). Local correlations are however often insufficient for regions with extremely sparse coverage, and these are quite common in scBS-seq data. Therefore, we share information across different cells by coupling the local GLM regressions through a shared prior distribution. In order to respect the (generally unknown) population structure that may be present within the cells assayed, we choose a (finite) Dirichlet mixture model prior.

The output of Melissa is therefore twofold: at each genomic region in each cell, we get a predicted profile of methylation, which can be used to impute missing data (i.e. unassayed CpGs). For each cell, we also get a discrete cluster membership probability, providing a methylome-based clustering of cells. This twofold output of Melissa reflects its methodological foundations as a hybrid between a global unsupervised model (Bayesian clustering of methylomes) and a local supervised learning model (GLM regression for every region). In this sense, Melissa is closer to a *mixture of experts* model (Bishop, 2006, Chapter 14, Section 5) than a standard mixture model.

2.1 Benchmarking Melissa on simulated data

We benchmark the ability of our model to cluster and impute CpG methylation states at the single cell level both on simulated and mouse embryonic stem cell (ESC) data sets. To assess test prediction performance we consider different metrics, including F-measure, the area under the receiver operating characteristic curve (AUC) and precision recall curves (Powers, 2011). We explore the performance of a number of methods as we vary three possible experimental parameters: the number of cells assayed, the cluster dissimilarity (how different the methylomes of cells in different

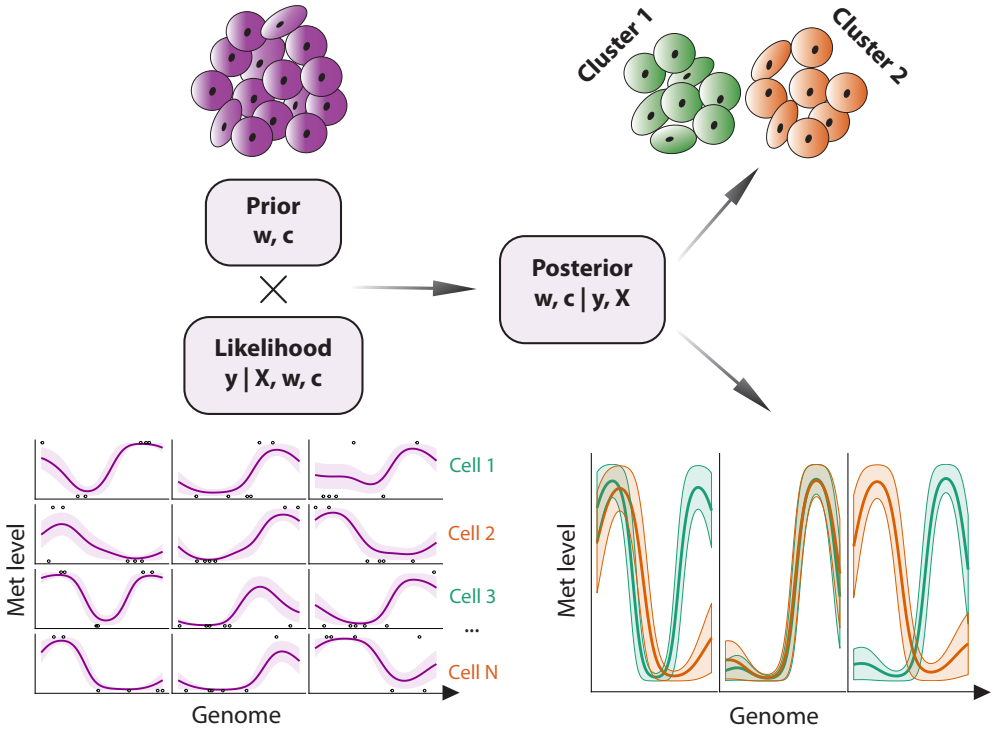

Figure 1: Melissa model overview. Melissa combines a likelihood computed from single cell methylation profiles fitted to each genomic region using a supervised regression approach (bottom left) and an unsupervised Bayesian clustering prior (top left). The posterior distribution provides a methylome-based clustering (top right) and imputation (bottom right) of single cells.

clusters are expected to be), and the CpG coverage (defined as the fraction of CpG sites covered by at least one read, averaged over all cells).

To benchmark the performance of *Melissa* in predicting CpG methylation states, we compare it against six different imputation strategies. As a baseline approach, we compute the average methylation rate separately for each cell and region (*Rate*), that is, the average is taken over all CpG sites forming a genomic region. We also use the BPRMeth model (Kapourani and Sanguinetti, 2016, 2018), where we account for the binary nature of the observations, which we train independently across cells and regions (*BPRMeth*). Note that BPRMeth shares information across CpG sites inside each genomic region, however, it does not transfer information across cells. To share information across cells, but not across neighbouring CpGs inside the region, we constrain Melissa to infer constant functions, i.e. learn average methylation rate (*Melissa rate*). We also use a Gaussian mixture model (*GMM*) that takes as input average M-values (Du *et al.*, 2010) instead of average methylation rates across the region (see "Methods" section); to avoid possible problems due to high-dimensionality, the GMM method was also tested on reduced-dimensionality data, where the first ten principal components were retained. Additionally, as a fully independent baseline, we use a Random Forest classifier trained on individual cells and regions, where the input features are the observed CpG locations, and the response variable is the CpG methylation state: methylated or unmethylated (*RF*). This is essentially the method of Zhang *et al.* (2015), however, without using additional annotation data or DNA sequence patterns. We delay comparisons with the deep learning method *DeepCpG* (Angermueller *et al.*, 2017) to the next section, as DeepCpG is not applicable in the settings of this simulation (see later Section 2.2 and 2.4).

In order to generate realistic simulated single-cell DNA methylation data, we extracted methylation profiles from real (bulk) BS-seq data using the BPRMeth package (Kapourani and Sanguinetti, 2018), and then generated binary methylation levels at a random subset of CpGs to simulate the low coverage of scBS-seq. In total we simulated $N = 200$ cells from $K = 4$ sub-populations, where each cell consisted of $M = 100$ genomic regions. Additionally, to account for different levels of similarity between cell sub-populations, we simulated 11 different datasets by varying the proportion of

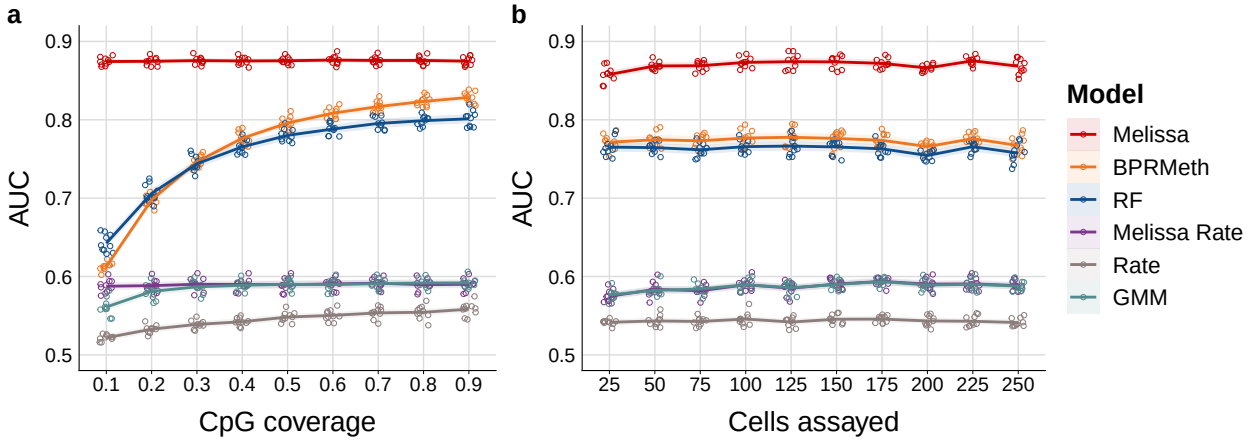

Figure 2: Melissa robustly imputes CpG methylation states. (**a**) Imputation performance in terms of AUC as we vary the proportion of covered CpGs used for training. Higher values correspond to better imputation performance. For each CpG coverage setting a total of 10 random splits of the data to training and test sets was performed. Each coloured circle corresponds to a different simulation. The plot shows also the LOESS curve for each method as we increase CpG coverage. The methods considered were: *Melissa* which shares information across cells and neighbouring CpGs, the *BPRMeth* model that only shares information across neighbouring CpGs, and a Random Forest classifier (*RF*) which predicts CpG methylation states using as input the observed CpG locations. Additionally, we considered three baseline models: *Melissa Rate* that transfers information across cells but not across neighbouring CpGs using mean methylation levels across the genomic region, a Gaussian mixture model (*GMM*) that takes as input average M-values across the region, and finally the *Rate* method where we compute a mean methylation rate separately for each cell and genomic region. (**b**) Imputation performance measured by AUC for varying number of cells assayed. In (**a**) N = 200 cells were simulated and cluster dissimilarity was set to 0.5, and in (**b**) CpG coverage was set to 0.4 and cluster dissimilarity to 0.5.

similar genomic regions between clusters. Finally, to assess the performance of Melissa as a function of assayed single cells we simulated 10 different datasets by varying N, the total number of single cells (see "Methods" section).

Applying the competing methods to synthetic data we observe that *Melissa* yields a substantial improvement in prediction accuracy compared to all other models (Fig. 2, Additional file 1: Fig. S1 and S2). Notably, *Melissa* is robust across different settings of the data, such as CpG coverage proportion (Fig. 2a) or the total number of cells assayed in each experiment (Fig. 2b). Due to its ability to transfer information across cells and neighbouring CpGs, our model robustly maintains its prediction accuracy at a very sparse coverage level of 10% or even when assaying around 25 single cells. The *BPRMeth* and *RF* models perform poorly at low CpG coverage settings, becoming comparable to *Melissa* when using the majority of the CpGs for training set. Importantly, *Melissa* still performs better at 90% CpG coverage, demonstrating that the clustering acts as an effective regularisation for imputing unassayed CpG sites. As expected, *Melissa Rate* and *GMM* have very similar performance (due to the very similar model structure); for both methods, performance is significantly weaker than *Melissa* across the full range of simulation settings, since they are not expressive enough to capture spatial correlations between CpGs. Using GMM on reduced dimensionality data did not lead to an improvement in performance, either for imputation or clustering (data not shown). Finally, the naive *Rate* method has the worst imputation performance of all methods, by a considerable margin. The imputation performance of all methods is relatively insensitive to the degree of cluster dissimilarity (Additional file 1: Fig. S2).

Next we consider the clustering performance of *Melissa*. Since most of the rival methods do not have a notion of clustering, we compare *Melissa* to clustering using methylation rates for binary data (*Melissa Rate*) or Gaussian data (*GMM*) using M-values (Du *et al.*, 2010). As a performance metric, we use the Adjusted Rand Index (ARI) (Hubert and Arabie, 1985) between the true cluster assignment and the predicted cluster membership returned from the model. Fig. 3a shows ARI values comparing the three models for varying CpG coverage (with cluster dissimilarity level at

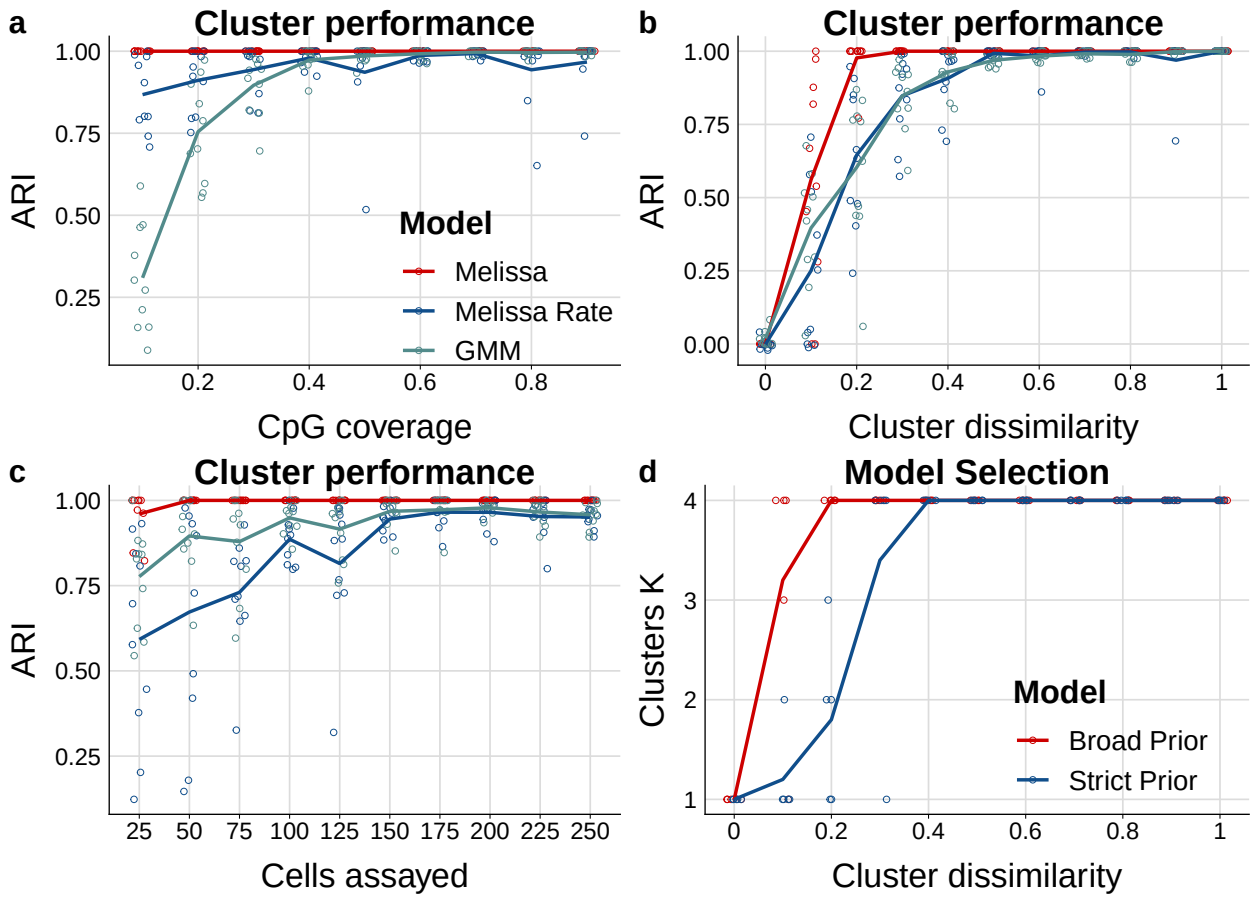

Figure 3: Melissa efficiently and accurately clusters cell sub-populations. (**a**) Clustering performance measured by ARI as we vary CpG coverage. Higher values correspond to better agreement between predicted and true cluster assignments. For each CpG coverage setting a total of 10 random splits of the data to training and test sets was performed. Each coloured circle corresponds to a different simulation. The plot shows also the LOESS curve for each method as we increase CpG coverage. (**b**) Clustering performance (ARI) for varying proportions of similar genomic regions between clusters. (**c**) Clustering performance (ARI) as we vary the total number of cells assayed. (**d**) Predicted number of clusters using two different prior settings: a broad and a strict prior as we vary cluster dissimilarity. Initial number of clusters was set to $K = 10$. Melissa identifies the correct number of clusters in most parameter settings ($K = 4$); notably when there is no dissimilarity across clusters (i.e. we have one global cell sub-population), Melissa prunes away all components and keeps only one cluster ($K = 1$).

0.5 and N = 200 cells). *Melissa* performs perfectly in all settings, demonstrating its power and sensitivity in identifying robustly the cell sub-population structure. When varying the level of cluster dissimilarity (see Fig. 3b), the model is still able to retain its high clustering performance. As expected, for settings with low variability between clusters (i.e. cell sub-populations are difficult to distinguish), the performance drops; however, *Melissa* is consistently superior to the *Melissa Rate* and *GMM* models, and rapidly reaches near-perfect clustering accuracy. Similarly, when varying the total number of cells assayed in each experiment (see Fig. 3c), Melissa retains its almost perfect clustering performance and is still consistently superior than the competing models.

Subsequently, we test *Melissa*'s ability to perform model selection, that is to identify the appropriate number of cell sub-populations. To do so, we run the model on simulated data, setting the initial number of clusters to K = 10 and letting the variational optimisation prune away inactive clusters (Corduneanu and Bishop, 2001). We used both broad (red line) and shrinkage (blue line) priors. Fig. 3d shows that the variational optimisation automatically recovered the correct number of mixture components for almost all parameter settings. As expected, in settings with high between cluster similarity, the model with shrinkage prior returned fewer clusters, since the data complexity term in Eq. (9) (see "Methods" section) was penalizing more the variational approximation com-

pared to the gain in likelihood from explaining the data. Finally, we assess the scalability of *Melissa* with respect to the number of single cells. Additional file 1: Fig. S3 compares the variational Bayes (red line) with the Gibbs sampling (blue line) algorithm; which demonstrates the good scalability of variational inference where we can analyse thousands of single cells in acceptable running times. The maximum number of iterations for the variational Bayes algorithm was set to 400 and the Gibbs algorithm was run for 3000 iterations. Both algorithms are implemented in the R programming language and were run on a machine utilising at most 16 CPU cores.

2.2 Benchmarking Melissa on subsampled bulk ENCODE data

The results in Section 2.1 convincingly showed a substantial advantage of *Melissa* over competing methods both in terms of imputation performance and in terms of clustering. However, conditioned on some seed profiles learnt from bulk data, the simulation was conducted on data which was directly sampled from the generative *Melissa* model (with some additional noise), which could conceivably introduce an unfair bias in the comparison. Additionally, since data were simulated as separate regions, comparison with the deep learning method DeepCpG (Angermueller *et al.*, 2017) was not possible, since DeepCpG requires the information of a large number of neighbouring CpGs to predict the methylation state of each target CpG site. To faithfully simulate scBS-seq data we generated two additional synthetic datasets by directly subsampling bulk ENCODE reduced representation bisulfite sequencing (RRBS) and whole genome bisulfite sequencing (WGBS) experiments (see "Methods" section). For the bulk RRBS data, we randomly subsampled 10% of the mapped reads and generated 40 pseudo-single cells from the GM12878 and H1-hESC cell lines. Due to the higher sequencing depth of bulk WGBS experiments, only 0.5% of the mapped reads were subsampled to generate pseudo-single cell methylomes. Subsequently, reads falling in the same genomic site were binarised to obtain a digital output of methylation. Finally, the two cell lines were combined in a single dataset of 80 pseudo-single cells prior to running Melissa. This procedure produces data with a more similar structure to real scBS-seq data, since the uneven read coverage better captures the structure of missing data observed in single cell epigenomic experiments.

Table 1 shows the results for the two studies when imputing CpGs falling in genomic regions of ±2.5 kb around transcription start sites (TSS) for different levels of CpG coverage. Consistently with the simulation study in Section 2.1, *Melissa* performs significantly better (on scRRBS synethtic data) or comparable (on scWGBS synthetic data) to competitors at imputation tasks. As reported in Angermueller *et al.* (2017), DeepCpG performs very strongly with comparable accuracy to *Melissa* across all CpG coverage settings (notice that training of DeepCpG is however slightly different, see "Methods" section). The systematically lower performance of DeepCpG on the scRRBS dataset is to be expected as DeepCpG relies on information from neighbouring CpGs over a large region,

	Pseudo scRRBS		Pseudo scWGBS	
Model	AUC 20% cov	AUC 50% cov	AUC 20% cov	AUC 50% cov
Melissa	**0.96** (7.3×10^{-4})	**0.96** (6.8×10^{-4})	**0.96** (6.3×10^{-4})	**0.96** (6.6×10^{-4})
DeepCpG	0.94 (1.5×10^{-3})	0.94 (1.5×10^{-3})	**0.96** (1.4×10^{-3})	**0.96** (1.4×10^{-3})
BPRMeth	0.88 (2.2×10^{-3})	0.91 (2.5×10^{-3})	0.90 (1.9×10^{-3})	0.92 (1.5×10^{-3})
RF	0.79 (3.2×10^{-3})	0.87 (2.0×10^{-3})	0.83 (2.2×10^{-3})	0.89 (2.1×10^{-3})
Melissa rate	0.88 (1.8×10^{-3})	0.88 (1.3×10^{-3})	0.70 (2.2×10^{-3})	0.71 (2.5×10^{-3})
Rate	0.82 (2.6×10^{-3})	0.84 (2.5×10^{-3})	0.76 (4.2×10^{-3})	0.77 (3.0×10^{-3})

Table 1: Melissa robustly imputes CpG methylation states on subsampled ENCODE scRRBS and scWGBS synthetic data. Imputation performance in terms of AUC as we vary the proportion of covered CpGs used for training. Higher values correspond to better imputation performance. For each CpG coverage setting a total of 10 random splits of the data to training and test sets was performed; shown are the mean AUC value together with two standard deviations of the estimate in parenthesis. Note that DeepCpG was trained once on two chromosomes, hence, the values do not change as we vary the CpG coverage.

and might therefore be at disadvantage for data generated using this technology. The results are consistent across all different metrics considered in this paper and when increasing the window size to ±5 kb around TSS (see Additional file 1: Fig. S4 - S9). Finally, Melissa could easily separate both cell sub-populations for all settings considered in this study.

2.3 Melissa accurately predicts methylation states on real data

To assess Melissa's performance on real scBS-seq data we considered two mouse ESC data sets from Angermueller *et al.* (2016) and Smallwood *et al.* (2014). The mouse ESCs were cultured either in 2i medium (*2i ESCs*) or serum conditions (*serum ESCs*), hence we expect methylation heterogeneity between cell sub-populations. In addition, in *serum ESCs* there is evidence of additional CpG methylation heterogeneity (Ficz *et al.*, 2013), making these data suitable for the model selection task to infer cell sub-population structure. The analysis on both data sets was performed on six different genomic contexts: protein coding promoters with varying genomic windows: ±1.5 kb, ±2.5 kb and ±5 kb around TSS, active enhancers, super enhancers and Nanog regulatory regions (see "Methods" section for details on data preprocessing). It should be noted that *DeepCpG* is designed to predict individual missing CpGs, rather than missing regions, and requires always information about neighbouring CpGs. This means that, during prediction, *DeepCpG* always has access to more data than competing methods, potentially providing it with an unfair advantage; to partly address this problem, we also present results when DeepCpG had access to subsampled data (labelled *DeepCpG Sub* in our figures). In general, *DeepCpG* should be thought as complementary to Melissa, and comparisons should be evaluated cautiously (see below Section 2.4).

We first applied *Melissa* on the Angermueller *et al.* (2016) data set which consists of 75 single cells (14 *2i ESCs* and 61 *serum ESCs*). Fig. 4a shows a direct comparison of the imputation performance of all the methods across a variety of genomic contexts. *Melissa* is better or comparable to rival methods in terms of AUC (see Fig. 4a), and substantially more accurate in terms of F-measure (Additional file 1: Fig. S10), demonstrating its ability to capture local CpG methylation patterns. *DeepCpG* also performs strongly on most genomic regions, indicating that a flexible deep learning method is effective in capturing patterns of methylation. Similar results were obtained by considering different metrics (Additional file 1: Fig. S10 - S12). Boxplots show performance distributions across 10 independent training / test splits of the data, except for *DeepCpG*, where the high computational costs prevented such investigation. Interestingly, methods based on methylation rates performed poorly at promoters, underlining the importance of methylation profiles in distinguishing epigenetic state near transcription start sites and identifying meaningful cell sub-populations. For all models, the imputation performance (in terms of AUC) at active enhancers was lower, indicating high methylation variability across cells and neighbouring CpG sites as shown in Smallwood *et al.* (2014).

In terms of clustering performance, *Melissa* confirms that the data supports the existence of a sub-population of serum cells as suggested in Ficz *et al.* (2013), by returning three clusters in almost all contexts. Further insights on the biological significance of the clusters obtained can be gleaned by inspecting the inferred methylation profiles at relevant regions. Fig. 4b shows posterior methylation profiles for three developmental genes for each cell sub-population (Additional file 1: Fig. S13 shows additional methylation profiles of developmental genes). Each colour corresponds to a different cell sub-population, with orange profiles corresponding to *2i ESCs* which are globally hypo-methylated. The green and purple profiles correspond to serum cells, which, as expected, present an increased level of methylation overall. However, *Melissa* identifies a clear sub-population structure within these serum cells: the purple cluster clearly represents a sub-population of cells which has only incompletely transitioned towards the final differentiated state (high global methylation punctuated by hypo-methylated CpG islands). Interestingly, 2i cells can be easily separated from serum cells based on methylation rate alone, due to the global hypo-methylation of 2i cells, however the sub-population structure within serum cells appears to be determined by changes in profiles.

As a second real data set, we analysed the smaller Smallwood *et al.* (2014) data set which consists of only 32 cells (12 *2i ESCs* and 20 *serum ESCs*). The imputation performance in terms of AUC across genomic contexts is shown in Fig. 5. Melissa retains its high prediction accuracy and is

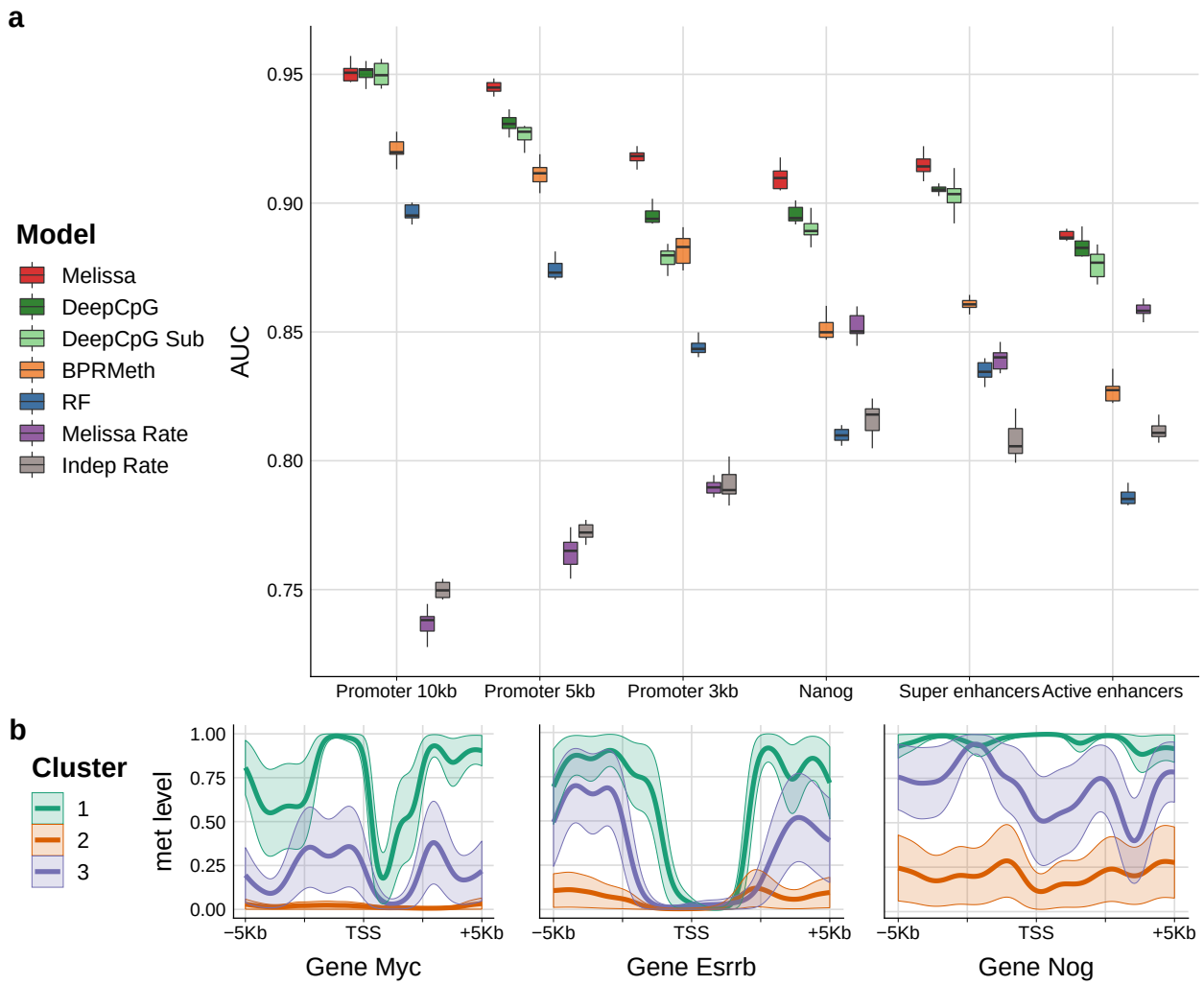

Figure 4: Imputation performance and clustering of mouse ESCs (Angermueller *et al.*, 2016) based on genome wide methylation profiles. **(a)** Prediction performance on test set for imputing CpG methylation states in terms of AUC. Higher values correspond to better imputation performance. Each coloured boxplot indicates the performance using 10 random splits of the data in training and test sets; due to high computational costs, DeepCpG was trained only once and the boxplots denote the variability across ten random subsamplings of the test set. **(b)** Example promoter regions with the predicted methylation profiles for three developmental genes: *Myc, Esrrb* and *Nog*. Each coloured profile corresponds to the average methylation pattern of the cells assigned to each sub-population, in our case Melissa identified $K = 3$ clusters.

comparable with DeepCpG across most contexts (see Additional file 1: Fig. S14 - S16 for performance on different metrics), even though the full DeepCpG model has slightly better performance on this data set. This suggests that the small number of cells in this data set did not allow an effective sharing of information. In terms of clustering performance, *Melissa* identifies three clusters in the vast majority of settings, once again underlying the emergence of epigenomically distinct populations within serum cells (see Additional file 1: Fig. S17 and S18 for example methylation profiles across genomic contexts).

2.4 A note on the comparison with DeepCpG

Melissa and DeepCpG models reported substantially better imputation performance compared to the rival methods and show comparable performance when analysed on real datasets, demonstrating their flexibility in capturing complex patterns of methylation. However, the two methods have significantly different computational performances. In our experiments, Melissa's runtime was less than six hours for all genomic contexts running on a small server machine utilising at most ten

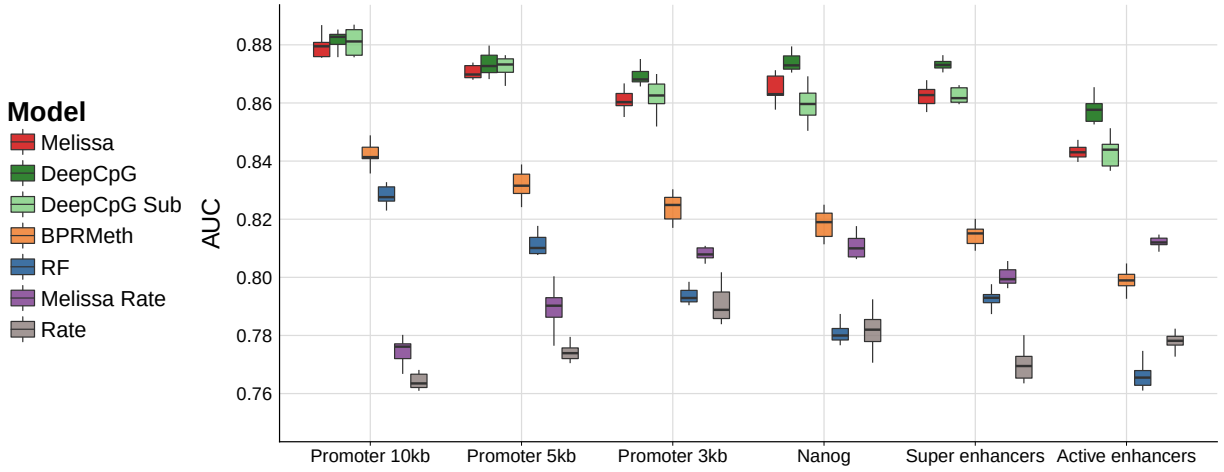

Figure 5: Imputation performance of mouse ESCs (Smallwood *et al.*, 2014) based on genome wide methylation profiles. Shown is the prediction performance, in terms of AUC, for imputing CpG methylation states. Each coloured boxplot indicates the performance using 10 random splits of the data in training and test sets; due to high computational costs, DeepCpG was trained only once and the boxplots denote the variability across ten random subsamplings of the test set.

CPU cores (see Additional file 1: Table S1 and S2). By contrast, DeepCpG required around three to four days to analyse each dataset on a GPU cluster equipped with high end NVIDIA Tesla K40ms GPUs, and had very high memory requirements. These computational overheads effectively make DeepCpG out of reach for smaller research groups. On the other hand, Melissa operates on a set of genomic contexts of interest (e.g. promoters), while DeepCpG is designed for genome-wide imputation; computational performance of both methods will therefore depend on specific choices, such as the size/ number of the regions of interest for Melissa, or the number of training chromosomes for DeepCpG.

In addition to the differences in scope between the two methods, one should also be cautious when directly comparing prediction performances due to the different design of the DeepCpG model. DeepCpG is trained on a specific set of chromosomes and considers each CpG site independently; hence it does not have a notion of genomic region to be trained on, and will in any case utilize information from neighbouring CpGs within or outside the region, information that Melissa and the rival methods do not have access to.

3 Conclusions

Single cell DNA methylation measurements are rapidly becoming a major tool to understand epigenetic gene regulation in individual cells. Newer platforms are rapidly expanding the scope of the technology in terms of assaying large numbers of cells (Luo *et al.*, 2017), however all technologies are plagued by intrinsically low coverage in terms of numbers of CpGs assayed.

In this paper, we have proposed Melissa as a way of addressing the low coverage issue by sharing information between CpGs with a local smoothing and between cells with a Bayesian clustering prior. On both synthetic and real data, Melissa achieved state of the art imputation performance over a panel of competing methods, including DeepCpG (Angermueller *et al.*, 2017) and random forests. While achieving comparable or superior performance to black-box methods, such as neural networks and random forests, Melissa is more transparent and needs minimal tuning: all the results shown, on both synthetic and real data, were obtained with the same settings of the algorithm. Additionally, as all Bayesian methods, Melissa outputs are probability distributions that fully quantify the uncertainty on the model's prediction, and which are more easily usable for further experimental design compared to the point-estimates provided by black-box approaches. Melissa does not require additional annotation data as in Zhang *et al.* (2015) or Ernst and Kellis (2015), and does

not exploit sequence information like DeepCpG, but an extension leveraging side data would be easily accomplished within the Bayesian framework and would represent an interesting extension for future research. By using a Bayesian clustering prior, Melissa has the added benefit of simultaneously uncovering the population structure within the assay, as we demonstrated in the real data examples; Melissa can therefore be a useful tool in uncovering epigenetic diversity among cells.

In addition, in this work Melissa was applied on pre-defined genomic regions of interest, such as promoters and enhancers, however, one could easily perform genome-wide imputation and clustering of single cell methylomes by using a sliding (non-overlapping) window approach. While this paper was under review, we became aware of a new preprint describing Epiclomal (de Souza *et al.*, 2018), a method to perform clustering of single cell DNA methylomes using a Bayesian probabilistic model. Epiclomal shares a similar hierarchical structure to Melissa, and also models bisulfite conversion error; however, Epiclomal does not model the spatial variability of neighbouring CpGs, and therefore cannot perform imputation as Melissa does.

While Melissa accounts for heterogeneity in the cell population structure, it does not allow for heterogeneity at the single gene level: each cluster has a single methylation profile within each region, and all variability at the single locus level is attributed to noise. This rigidity limits the usefulness of Melissa as a tool to investigate intrinsic stochasticity in methylation at the single locus level. Relaxing the modelling assumptions to accommodate methylation variability in Melissa is an interesting topic for future research. Another area where Melissa could be fruitfully applied is the integrative study of multiple high-throughput features in single cells. Kapourani and Sanguinetti (2016) showed that features extracted from methylation profiles could be effectively used to predict gene expression in bulk experiments. With the advent of novel technologies measuring gene expression and multiple epigenomic features in individual cells (Clark *et al.*, 2018), interpretable Bayesian models like Melissa are likely to play an important role in furthering our understanding of epigenetic control of gene expression in single cells.

4 Methods

4.1 Melissa model

In order to provide spatial smoothing of the methylation profiles at specific regions, we adapt a generalised linear model of basis function regression proposed recently in Kapourani and Sanguinetti (2016) and further extended and implemented in the BPRMeth Bioconductor package in (Kapourani and Sanguinetti, 2018). The basic idea of BPRMeth is as follows: the methylation profile associated with a genomic region m is defined as a (latent) function $f\colon m \rightarrow (0, 1)$ which takes as input the genomic coordinate along the region and returns the propensity for that locus to be methylated. For single-cell methylation data, methylation of individual CpG sites can be naturally modelled using a Bernoulli observation model, since for the majority of covered sites we have binary CpG methylation states (see Additional file 1: Fig. S13). More specifically, for a specific region m, we model the observed methylation of CpG site i as

$$y_{mi} \sim \mathcal{B}\text{ern}(\rho_{mi}), \tag{1}$$

where the unknown "true" methylation level ρ_{mi} has as covariates the CpG locations x_{mi}. Then, we define the BPRMeth model as

$$\begin{aligned} \eta_{mi} &= \mathbf{w}_m^\top \mathbf{h}(x_{mi}), \\ f_m(x_{mi}) &= \rho_{mi} = g^{-1}(\eta_{mi}), \end{aligned} \tag{2}$$

where $\mathbf{w}_m$ are the regression coefficients, $\mathbf{x}_{mi} \equiv \mathbf{h}(x_{mi})$ are the basis function transformed CpG locations (here we consider radial basis functions (RBFs)), and $g(\cdot)$ is the link function that allows us to move from the systematic components η_{mi} to mean parameters ρ_{mi}. Here we consider a *probit regression* model which is obtained by defining $g^{-1}(\cdot) = \Phi(\cdot)$ — where $\Phi(\cdot)$ denotes the cdf of the standard normal distribution — ensuring that f takes values in the $[0, 1]$ interval. Notice that both

BPRMeth and *Melissa* do not explicitly model bisulfite conversion errors. Conversion errors are estimated to be relatively rare and below 1% according to Genereux *et al.* (2008), and we show in our simulation studies that *Melissa* is highly robust to the addition of noise mimicking possible errors.

To account for the limited CpG coverage of scBS-seq experiments, the BPRMeth model was recently reformulated in a Bayesian framework (Kapourani and Sanguinetti, 2018). The model was made amenable to Bayesian estimation thanks to a data augmentation strategy originally proposed by Albert and Chib (1993). This strategy consists of introducing an additional auxiliary latent variable z_i, which has a Gaussian distribution conditioned on the input $\mathbf{w}^\top \mathbf{x}_i$, leading to the graphical model in Fig. 6.

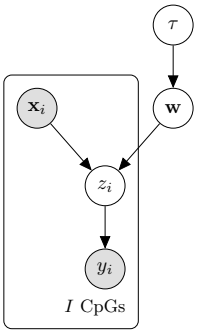

$$
\begin{aligned}
\tau &\sim \mathcal{G}\text{amma}(\tau \,|\, \alpha_0, \beta_0) \\
\mathbf{w} \,|\, \tau &\sim \mathcal{N}(\mathbf{w} \,|\, \mathbf{0}, \tau^{-1}\mathbf{I}) \\
z_i \,|\, \mathbf{w}, \mathbf{x}_i &\sim \mathcal{N}(z_i \,|\, \mathbf{w}^\top \mathbf{x}_i, 1) \\
y_i \,|\, z_i &= \begin{cases} 1 & \text{if } z_i > 0 \\ 0 & \text{if } z_i \leq 0 \end{cases}
\end{aligned}
$$

Figure 6: Probabilistic graphical representation of the BPRMeth model.

The BPRMeth model is limited to sharing information across CpGs via local smoothing (which certainly helps in dealing with data sparsity), however, in our experience the coverage in scBS-seq data is insufficient to infer informative methylation profiles at many genomic regions. We therefore propose Melissa to exploit the population structure of the experimental design and additionally share and transfer information across cells.

Assume that we have $N(n = 1, ..., N)$ cells and each cell consists of $M(m = 1, ..., M)$ genomic regions, for example promoters, and we are interested in both partitioning the cells in K clusters and inferring the methylation profiles for each genomic region. To do so, we use a finite Dirichlet mixture model (FDMM) (McLachlan and Peel, 2004), where we assume that the methylation profile of the m^{th} region for each cell n is drawn from a mixture distribution with K components (where $K < N$). This way cells belonging to the same cluster will share the same methylation profile, although profiles will still differ across genomic regions. Let $\mathbf{c}_n$ be a latent variable comprising a 1-of-K binary vector with elements c_{nk} representing the component that is responsible for cell n, and π_k be the probability that a cell belongs to cluster k, i.e. $\pi_k = p(c_{nk} = 1)$. The conditional distribution of $\mathbf{C} = \{\mathbf{c}_1, \ldots, \mathbf{c_N}\}$ given $\boldsymbol{\pi}$ is

$$
p(\mathbf{C} \,|\, \boldsymbol{\pi}) = \prod_{n=1}^{N} \prod_{k=1}^{K} \pi_k^{c_{nk}}. \tag{3}
$$

Considering the FDMM as a generative model, the latent variables $\mathbf{c}_n$ will generate the latent observations $\mathbf{Z}_n \in \mathbb{R}^{M \times I_m}$, which in turn will generate the binary observations $\mathbf{Y}_n \in \{0, 1\}^{M \times I_m}$ depending on the sign of $\mathbf{Z}_n$, as shown in Fig. 6. The conditional distribution of the data $(\mathbf{Z}, \mathbf{Y})$, given the latent variables $\mathbf{C}$ and the component parameters $\mathbf{W}$ becomes

$$
p(\mathbf{Y}, \mathbf{Z} \,|\, \mathbf{C}, \mathbf{W}, \mathbf{X}) = \prod_{n=1}^{N} \prod_{k=1}^{K} \left[\prod_{m=1}^{M} p(\mathbf{y}_{nm} \,|\, \mathbf{z}_{nm})\, p(\mathbf{z}_{nm} \,|\, \mathbf{w}_{mk}, \mathbf{X}_{nm}) \right]^{c_{nk}}, \tag{4}
$$

where

$$
p(\mathbf{y}_{nm} \,|\, \mathbf{z}_{nm}) = \mathbb{I}(\mathbf{z}_{nm} > 0)^{\mathbf{y}_{nm}} \mathbb{I}(\mathbf{z}_{nm} \leq 0)^{(\mathbf{1} - \mathbf{y}_{nm})}.
$$

To complete the model we introduce priors over the parameters. We choose a Dirichlet distribution over the mixing proportions, $p(\boldsymbol{\pi}) = \mathcal{D}\text{ir}(\boldsymbol{\pi} \,|\, \boldsymbol{\delta}_0)$, where for symmetry we choose the same parameter

δ_{0_k} for each of the mixture components. We also introduce an independent Gaussian prior over the coefficients $\mathbf{W}$, that is,

$$p(\mathbf{W} \mid \boldsymbol{\tau}) = \prod_{m=1}^{M} \prod_{k=1}^{K} \mathcal{N}(\mathbf{w}_{mk} \mid \mathbf{0}, \tau_k^{-1}\mathbf{I}). \tag{5}$$

Finally, we introduce a prior distribution for the (hyper)-parameter $\boldsymbol{\tau}$, and assume that each cluster has its own precision parameter, $p(\tau_k) = \mathcal{G}\text{amma}(\tau_k \mid \alpha_0, \beta_0)$. Having defined our model, we can now write the joint distribution over the observed and latent variables

$$p(\mathbf{Y}, \mathbf{Z}, \mathbf{C}, \mathbf{W}, \boldsymbol{\pi}, \boldsymbol{\tau} \mid \mathbf{X}) = p(\mathbf{Y} \mid \mathbf{Z})\, p(\mathbf{Z} \mid \mathbf{C}, \mathbf{W}, \mathbf{X})\, p(\mathbf{C} \mid \boldsymbol{\pi})\, p(\boldsymbol{\pi})\, p(\mathbf{W} \mid \boldsymbol{\tau})\, p(\boldsymbol{\tau}), \tag{6}$$

where the factorisation corresponds to the probabilistic graphical model shown in Fig. 7.

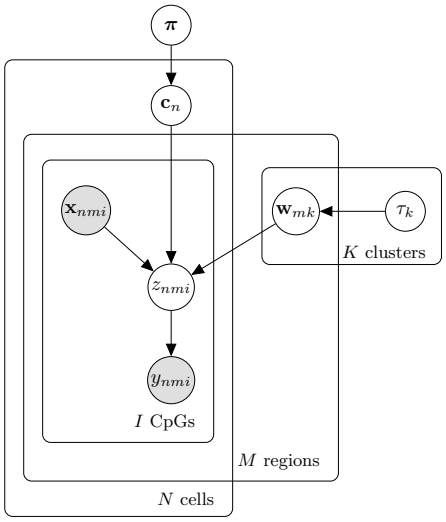

$$\begin{aligned}
\boldsymbol{\pi} &\sim \mathcal{D}\text{ir}(\boldsymbol{\delta}_0) \\
\mathbf{c}_n \mid \boldsymbol{\pi} &\sim \mathcal{D}\text{iscrete}(\boldsymbol{\pi}) \\
\tau_k &\sim \mathcal{G}\text{amma}(\alpha_0, \beta_0) \\
\mathbf{w}_{mk} \mid \tau_k &\sim \mathcal{N}(\mathbf{0}, \tau_k^{-1}\mathbf{I}) \\
z_{nmi} \mid \mathbf{w}_{mk}, \mathbf{x}_{nmi} &\sim \mathcal{N}(\mathbf{w}_{mk}^{\top}\mathbf{x}_{nmi}, 1) \\
y_{nmi} \mid z_{nmi} &= \begin{cases} 1 & \text{if } z_{nmi} > 0 \\ 0 & \text{if } z_{nmi} \leq 0 \end{cases}
\end{aligned}$$

Figure 7: Probabilistic graphical representation of the Melissa model.

Importantly, Melissa is a hybrid between a global unsupervised clustering model and a local supervised prediction model, encoded through the GLM regression coefficients $\mathbf{w}$ for each genomic region. When considering Melissa as an imputation (or predictive) model, the training data are coming by using only a subset of CpG tuples (x_{nmi}, y_{nmi}) for each region. For example, from the observed I_{nm} CpGs in a given region, Melissa will only see $I_{nm}/2$ random CpGs during training, and the remaining CpGs will be used as a held out test set to evaluate its prediction performance. Note that in any case, either using all CpGs or a subset during training, Melissa will additionally perform clustering at the global level which is encoded through the latent variables $\mathbf{c}_n$.

Variational Inference

The posterior distribution of the latent variables given the observed data $p(\mathbf{Z}, \mathbf{C}, \mathbf{W}, \boldsymbol{\pi}, \boldsymbol{\tau} \mid \mathbf{Y}, \mathbf{X})$ for the Melissa model is not analytically tractable; hence, we resort to approximate techniques. The most common method for approximate Bayesian inference is to perform Markov Chain Monte Carlo (MCMC) (Gelfand and Smith, 1990), however, sampling methods require considerable computational resources and do not scale well when performing genome-wide analysis on hundreds or thousands of single cells. Variational methods can provide an efficient, approximate solution with better scalability in this case (see "Results" section for a comparison between Gibbs sampling and variational inference for this model). More specifically, we use mean-field variational inference (Blei *et al.*, 2017) which assumes that the approximating distribution factorises over the latent variables,

$$q(\mathbf{Z}, \mathbf{C}, \mathbf{W}, \boldsymbol{\pi}, \boldsymbol{\tau}) = q(\mathbf{Z})\, q(\mathbf{C})\, q(\mathbf{W})\, q(\boldsymbol{\pi})\, q(\boldsymbol{\tau}). \tag{7}$$

Detailed mathematical derivations of the optimal variational factors are available in Additional file 1: Section 1. Next we iteratively update each factor q while holding the remaining factors fixed using the coordinate ascent variational inference (CAVI) algorithm which is summarised in Algorithm 1.

Algorithm 1 CAVI for Melissa model

initialize Gaussian factor $\boldsymbol{\lambda}, \mathbf{S}$; Dirichlet factor $\boldsymbol{\delta_0}$; and Gamma factor α_0, β_0.
Update $\alpha_k \leftarrow \alpha_0 + MD/2$
Update $\beta_k \leftarrow \beta_0$
while ELBO has not converged **do**
    Set $\gamma_{nmk} = (\mathbf{z}_{nm} - \mathbf{X}_{nm}\mathbf{w}_{mk})$ ▷ **Variational E-step**
    Update $r_{nk} \propto \langle \ln \pi_k \rangle_{q(\pi_k)} + \sum_m \left\langle -\frac{1}{2}\gamma_{nmk}^\top \gamma_{nmk} \right\rangle_{q(\mathbf{z}_{nm}, \mathbf{w}_{mk})}$
    ▷ **Variational M-step**
    Update $\delta_k \leftarrow \delta_{0_k} + \sum_n r_{nk}$ ▷ Dirichlet distribution parameter
    Update $\beta_k \leftarrow \beta_0 + \frac{1}{2}\sum_m \left\langle \mathbf{w}_{mk}^\top \mathbf{w}_{mk} \right\rangle_{q(\mathbf{w}_{mk})}$ ▷ Gamma distribution parameter
    Update $\mu_{nmi} \leftarrow \sum_k r_{nk} \left\langle \mathbf{w}_{mk}^\top \mathbf{x}_{nmi} \right\rangle_{q(\mathbf{w}_{mk})}$ ▷ Mean of truncated Gaussian
    Set $\langle z_{nmi} \rangle_{q(z_{nmi})} = \begin{cases} \mu_{nmi} + \phi(-\mu_{nmi}) / \big(1 - \Phi(-\mu_{nmi})\big) & \text{if } y_{nmi} = 1 \\ \mu_{nmi} - \phi(-\mu_{nmi}) / \Phi(-\mu_{nmi}) & \text{if } y_{nmi} = 0 \end{cases}$
    Update $\mathbf{S}_{mk} \leftarrow \left(\frac{\alpha_k}{\beta_k}\mathbf{I} + \sum_n r_{nk} \mathbf{X}_{nm}^\top \mathbf{X}_{nm} \right)^{-1}$ ▷ Regression coefficient covariance
    Update $\boldsymbol{\lambda}_{mk} \leftarrow \mathbf{S}_{mk} \sum_n r_{nk} \mathbf{X}_{nm}^\top \langle \mathbf{z}_{nm} \rangle_{q(\mathbf{z}_{nm})}$ ▷ Regression coefficient mean
    Update $\mathcal{L}\left(q(\mathbf{W}, \mathbf{Z}, \mathbf{C}, \boldsymbol{\pi}, \boldsymbol{\tau})\right)$ ▷ Compute ELBO
end while

Predictive density and model selection

Given an approximate posterior distribution, we are in the position to predict the methylation level at unobserved CpG sites. The predictive density of a new observation $\mathbf{y}_*$, which is associated with latent variables $\mathbf{c}_*$, $\mathbf{z}_*$ and covariates $\mathbf{X}_*$, is given by

$$\begin{aligned} p(\mathbf{y}_* \,|\, \mathbf{X}_*, \mathbf{Y}) &= \sum_{c_*} \int \int p(\mathbf{y}_*, \mathbf{c}_*, \mathbf{z}_*, \boldsymbol{\theta} \,|\, \mathbf{X}_*, \mathbf{Y}) d\boldsymbol{\theta} d\mathbf{z}_* \\ &\simeq \sum_{k=1}^{K} \frac{\delta_k}{\sum_j \delta_j} \mathcal{B}\text{ern}\left(\mathbf{y}_* \middle| \Phi\left(\frac{\mathbf{X}_* \boldsymbol{\lambda}_k}{\sqrt{\mathbf{I} + \text{diag}\big(\mathbf{X}_* \mathbf{S}_k \mathbf{X}_*^T\big)}} \right) \right) \end{aligned} \tag{8}$$

where we collectively denote as $\boldsymbol{\theta}$ the relevant parameters being marginalised.

It has been repeatedly observed (Corduneanu and Bishop, 2001) that, when fitting variationally a mixture model with a large number of components, the variational procedure will prune away components with no support in the data, hence effectively determining an appropriate number of clusters in an automatic fashion, i.e. perform model selection. We can gain some intuition as to why this happens in the following way. We can rewrite the Kullback-Leibler ($\mathcal{KL}$) divergence as

$$\mathcal{KL}(q(\boldsymbol{\theta}) \,||\, p(\boldsymbol{\theta} \,|\, \mathbf{X})) = \ln p(\mathbf{X}) - \langle \ln p(\mathbf{X} \,|\, \boldsymbol{\theta}) \rangle_{q(\boldsymbol{\theta})} + \mathcal{KL}(q(\boldsymbol{\theta}) \,||\, p(\boldsymbol{\theta})) \tag{9}$$

where $\ln p(\mathbf{X})$ can be ignored since is constant with respect to $q(\boldsymbol{\theta})$. To minimize this objective function the variational approximation will both try to increase the expected log likelihood of the data $\ln p(\mathbf{X} \,|\, \boldsymbol{\theta})$ while minimizing its $\mathcal{KL}$ divergence with the prior distribution $\text{p}(\boldsymbol{\theta})$. Hence, using variational Bayes we have an automatic trade-off between fitting the data and model complexity (Bishop, 2006).

4.2 Assessing Melissa via a simulation study

To generate realistic simulated single-cell methylation data, we first used the BPRMeth package (Kapourani and Sanguinetti, 2018) to infer five prototypical methylation profiles from the GM12878 lymphoblastoid cell line. The bulk BS-seq data for the GM12878 cell line are publicly

available from the ENCODE project (Dunham *et al.*, 2012). Based on these profiles we simulated single cell methylation data (i.e. binary CpG methylation states) for M = 100 genomic regions, where each CpG was generated by sampling from a Bernoulli distribution with probability of success given by the latent function evaluation at the specific site. To mimic the inherent noise introduced by bisulfite conversion error, Gaussian noise $\mathcal{N}(\mu = 0, \sigma = 0.05)$ was introduced to the probability of success prior to generating each binary CpG site. This process can be thought of as generating methylation data for a specific single cell. Next, we generated K = 4 cell sub-populations by randomly shuffling the genomic regions across clusters, so now each cell sub-population has its own methylome landscape. In total we generated N = 200 cells, with the following cell sub-population proportions: 40%, 25%, 20% and 15%. Additionally, to account for different levels of similarity between cell sub-populations, we simulated 11 different datasets by varying the proportion of similar genomic regions between clusters. Finally, to assess the performance of Melissa for varying number of cells assayed we simulated 10 different datasets by varying the total number of single cells N. The scripts (written in the R programming language) for this simulation study are publicly available on the Melissa repository.

4.3 Assessing Melissa on subsampled bulk ENCODE data

To faithfully simulate methylation data that resemble scBS-seq experiments, we generated two additional synthetic datasets by subsampling bulk ENCODE RRBS (GEO: GSE27584) and WGBS (GEO: GSE80911 for H1-hESC and GSE86765 for GM12878) data, each consisting of two different cell lines, H1-hESC and GM12878. The RRBS data are enriched for genomic regions with high CpG content (using methylation sensitive restriction enzymes such as *MspI* that recognises CCGG motifs) which predominantly reside near promoter regions and CpG islands. On the other hand, WGBS experiments in theory can assay the whole methylome landscape of the human genome, however, they require high sequencing depth to obtain an accurate estimate of the bulk methylation level at each CpG site. To retain the structure of missing data observed in scBS-seq experiments (due to read length), we directly subsampled the raw FASTQ files which essentially lead to discarding individual reads rather than individual CpGs. For the RRBS dataset, from each cell line we generated 40 pseudo-single cells by randomly keeping 10% of the mapped reads from the bulk experiment, resulting in 80 cells when combining both cell lines. For the WGBS dataset, the same number of pseudo-single cells was generated from each cell line, with the only difference that only 0.5% of the mapped reads were retained from the bulk data due to the high sequencing depth of the experiments. This process was performed for chromosomes 1 to 6 to alleviate the computational burden. Subsequently, the same preprocessing steps detailed in Section 4.4 were performed, with the only difference that for this study we considered only ±2.5 kb and ±5 kb promoter regions around TSS. Each model, except DeepCpG, used 20%, 50% and 80% of the CpGs as training set, and the remaining of CpGs were used as a test set to evaluate imputation performance. The DeepCpG model used chromosomes 1 and 3 as training set, chromosome 5 as validation set and the remaining chromosomes as test set.

4.4 scBS-seq data and preprocessing

Single cell bisulfite sequencing protocols provide us with single base-pair resolution of CpG methylation states. Since we assay the DNA of a single cell, the methylation level for each CpG site is predominantly binary, either methylated or unmethylated. However, due to each chromosome having two copies, a small proportion of CpG sites have a non-binary nature (see Additional file 1: Fig. S19). To avoid ambiguities, hemi-methylated sites — sites with 50% methylation level — are filtered prior to downstream analysis, and for the remaining sites binary methylation states are obtained from the ratio of methylated read counts to total read counts, in a similar fashion to Angermueller *et al.* (2016).

Two mouse embryonic stem cells (ESCs) datasets were used to validate the performance of the Melissa model. The first dataset presented in Angermueller *et al.* (2016), after quality assessment,

consisted of 75 single cells out of which 14 cells were cultured in 2i medium (*2i ESCs*) and the remaining 61 cells were cultured in serum conditions (*serum ESCs*). The Bismark (Krueger and Andrews, 2011) processed data, with reads mapped to the GRCm38 mouse genome, were downloaded from the Gene Expression Omnibus under accession GSE74535. The second dataset (Smallwood *et al.*, 2014) contained 32 cells out of which 12 cells were *2i ESCs* and the remaining 20 cells were *serum ESCs* and the Bismark processed data, with reads mapped to the GRCm38 mouse genome, are publicly available under accession number GSE56879. For both datasets, the observed data that are used as input to Melissa, are binary methylation states: unmethylated CpGs are encoded with zero and methylated CpGs with one. We should note that this is the standard procedure for processing scBS-seq data (Smallwood *et al.*, 2014) and additional information and visualisations regarding the quality of the scBS-seq data can be found in the original publications.

Since Melissa considers genomic regions for a specific genomic context, we use the BPRMeth package (Kapourani and Sanguinetti, 2018) to filter CpGs that do not fall inside these regions, and create a simple data structure where each cell is a encoded as a list, and each entry of the list — corresponding to a specific genomic region — is a matrix with two columns: the (relative) CpG location and the methylation state. We considered six different genomic contexts where we applied Melissa: protein coding promoters with varying genomic windows: ± 1.5 kb, ± 2.5 kb and ± 5 kb around transcription start sites (TSS), active enhancers, super enhancers and Nanog regulatory regions. Due to the sparse CpG coverage, for the three genomic contexts except promoters we filtered loci with smaller than 1 kb annotation length and specifically for Nanog regions we took a window of ± 2.5 kb around the centre of the genomic annotation. In addition, we only considered regions that were covered in at least 50% of the cells with a minimum coverage of 10 CpGs and had between cell variability; the rationale being that homogeneous regions across cells do not provide additional information for identifying cell sub-populations. The CpG coverage distribution after the filtering process across different genomic contexts is shown in Additional file 1: Fig. S20 and S21. The sparsity level of the two scBS-seq datasets across different genomic contexts is shown in Additional file 1: Table S3. It should be noted, that imputation performance is evaluated only on genomic regions that pass the filtering threshold. We run the model with $K = 6$ and $K = 5$ clusters for the Angermueller *et al.* (2016) and Smallwood *et al.* (2014) datasets, respectively, and we use a broad prior over the model parameters.

4.5 Performance evaluation

To assess model performance across all genomic contexts, we partition the data and use 50% of the CpGs in each cell and region for training set and the remaining 50% as test set (except DeepCpG, see below). The prediction performance of all competing models, except DeepCpG, was evaluated on imputing all missing CpG states in a given region at once. For computing binary evaluation metrics, such as F-measure, predicted probabilities above 0.5 were set to one and rounded to zero otherwise.

F-measure The F-measure or F_1-score is the harmonic mean of precision and recall:

$$F\text{-measure} = 2 \cdot \frac{\text{precision} \cdot \text{recall}}{\text{precision} + \text{recall}}. \tag{10}$$

Gaussian mixture model The input to the Gaussian mixture model (GMM) is the average methylation rate across the region; since rates are between (0,1) we transform them to M-values, which follow closer the Gaussian distribution (Du *et al.*, 2010). The transformation from average methylation rates to average M-values is obtained by

$$M\text{-value} = \log_2 \left(\frac{\text{rate} + 0.01}{1 - \text{rate} + 0.01} \right). \tag{11}$$

Adjusted Rand Index The Adjusted Rand Index (ARI) is a measure of the similarity between two data clusterings:

$$ARI = \frac{\sum_{ij}\binom{n_{ij}}{2} - \left[\sum_i \binom{\alpha_i}{2}\sum_j \binom{\beta_j}{2}\right]/\binom{n}{2}}{\frac{1}{2}\left[\sum_i \binom{\alpha_i}{2} + \sum_j \binom{\beta_j}{2}\right] - \left[\sum_i \binom{\alpha_i}{2}\sum_j \binom{\beta_j}{2}\right]/\binom{n}{2}}. \tag{12}$$

DeepCpG

The DeepCpG method takes a different imputation approach: it is trained on a specific set of chromosomes and predicts methylation states on the remaining chromosomes where it imputes each CpG site sequentially by using as input a set of neighbouring CpG sites. This approach makes it difficult to equally compare with the rival methods, since for each CpG the input features to DeepCpG are all the neighbouring sites, whereas the competing models have access to a subset of the data and they make predictions in one pass for the whole region. Since we only had access to CpG methylation data and to make it comparable with the considered methods, we trained the CpG module of DeepCpG (termed *DeepCpG CpG* in Angermueller *et al.* (2017)).

For the Angermueller *et al.* (2016) dataset, chromosomes 3 and 17 were used as training set, chromosomes 12 and 14 as validation set and the remaining chromosomes as test set. For the Smallwood *et al.* (2014) dataset, chromosomes 3, 17 and 19 were used as training set, chromosomes 12 and 14 as validation set and the remaining chromosomes as test set. The chosen chromosomes had at least 3 million CpGs used as training set; a sensible size for the DeepCpG model as suggested by the authors. A neighbourhood of K = 20 CpG sites to the left and the right for each target CpG was used as input to the model. During testing time, even if a given genomic region did not contain at least 40 CpGs, the DeepCpG model used additional CpGs outside this window to predict methylation states; hence using more information compared to the rival models. In total the DeepCpG model took around four days per dataset for training and prediction on a cluster equipped with NVIDIA Tesla K40ms GPUs.

Abbreviations

ARI: Adjusted rand index; AUC: Area under the receiver operating characteristic curve; BPRMeth: Bayesian probit regression for methylation; bp: Base pair; CAVI: Coordinate ascent variational inference; CPU: Central processing unit; ESC: Embryonic stem cell; GEO: Gene Expression Omnibus; GLM: Generalised linear model; GMM: Gaussian mixture model; GPU: Graphics processing unit; MCMC: Markov chain Monte Carlo; RBF: Radial basis function; RF: Ranfom forest; scBS-seq: Single-cell bisulfite sequencing; scRRBS: Single-cell reduced representation bisulfite sequencing; TSS: Transcription start site; WGBS: Whole genome bisulfite sequencing.

Declarations

Acknowledgements

We thank Duncan Sproul and Jon Higham for discussion and help with bioinformatics pipeline analysis and Oliver Stegle, Michalis Michaelides, Ricard Argelaguet, and Stephen Clark for valuable comments and discussion.

Funding

CAK is a cross-disciplinary post-doctoral fellow supported by funding from the University of Edinburgh, Medical Research Council (core grant to the MRC Institute of Genetics and Molecular Medicine), and the EPSRC Centre for Doctoral Training in Data Science, funded by the UK Engineering and Physical Sciences Research Council (grant EP/L016427/1).

Availability of data and materials

The Melissa model is publicly available as R software (https://github.com/andreaskapou/Melissa, doi: 10.5281/zenodo.2567427) released under GNU GPL-3 licence. The scBS-seq data from mouse ESCs from Smallwood *et al.* (2014) are available under GEO accession number GSE56879. The scM&T-seq data from mouse ESCs from Angermueller *et al.* (2016) are available under GEO accession number GSE74535.

Authors' contributions

Both authors conceived the study, carried out the data analysis, and wrote the paper. CAK implemented and evaluated the method. Both authors read and approved the final manuscript.

Authors' information

Correspondence and requests for materials should be addressed to
C.A.Kapourani@ed.ac.uk or G.Sanguinetti@ed.ac.uk.

Competing interests

The authors declare that they have no competing interests.

Ethics approval and consent to participate

Ethical approval was not needed for this study.

Consent for publication

Not applicable.

Additional files

Additional file 1: Melissa mean-field variational inference derivations (section 1), additional figures (section 2), and additional tables (section 3). (PDF 884.3 kB)

References

Albert, J. H. and Chib, S. (1993). Bayesian Analysis of Binary and Polychotomous Response Data. *Journal of the American Statistical Association*, **88**(422), 669–679.

Angermueller, C., Clark, S. J., Lee, H. J., Macaulay, I. C., Teng, M. J., Hu, T. X., Krueger, F., Smallwood, S. A., Ponting, C. P., Voet, T., Kelsey, G., Stegle, O., and Reik, W. (2016). Parallel single-cell sequencing links transcriptional and epigenetic heterogeneity. *Nature methods*, **13**(3), 229–32.

Angermueller, C., Lee, H. J., Reik, W., and Stegle, O. (2017). DeepCpG: accurate prediction of single-cell DNA methylation states using deep learning. *Genome Biology*, **18**(1), 67.

Baylin, S. B. and Jones, P. a. (2011). A decade of exploring the cancer epigenome - biological and translational implications. *Nature Reviews Cancer*, **11**(10), 726–734.

Bird, A. (2002). DNA methylation patterns and epigenetic memory. *Genes and Development*, **16**(1), 6–21.

Bishop, C. M. (2006). *Pattern recognition and machine learning*. Springer.

Blei, D. M., Kucukelbir, A., and McAuliffe, J. D. (2017). Variational Inference: A Review for Statisticians. *Journal of the American Statistical Association*, **112**(518), 859–877.

Clark, S. J., Argelaguet, R., Kapourani, C. A., Stubbs, T. M., Lee, H. J., Alda-Catalinas, C., Krueger, F., Sanguinetti, G., Kelsey, G., Marioni, J. C., Stegle, O., and Reik, W. (2018). ScNMT-seq enables joint profiling of chromatin accessibility DNA methylation and transcription in single cells. *Nature Communications*, **9**(1), 1–9.

Corduneanu, A. and Bishop, C. M. (2001). Variational Bayesian Model Selection for Mixture Distributions. *In Artificial Intelligence and Statistics*, pages 27–34.

de Souza, C. P. E., Andronescu, M., Masud, T., Kabeer, F., Biele, J., Laks, E., Lai, D., Brimhall, J., Wang, B., Su, E., Hui, T., Cao, Q., Wong, M., Moksa, M., Moore, R. A., Hirst, M., Aparicio, S., and Shah, S. P. (2018). Epiclomal: probabilistic clustering of sparse single-cell DNA methylation data. *bioRxiv*, page 414482.

Du, P., Zhang, X., Huang, C. C., Jafari, N., Kibbe, W. A., Hou, L., and Lin, S. M. (2010). Comparison of Beta-value and M-value methods for quantifying methylation levels by microarray analysis. *BMC Bioinformatics*, **11**(1), 587.

Dunham, I., Kundaje, A., and Encode Project Consortium (2012). An integrated encyclopedia of DNA elements in the human genome. *Nature*, **489**(7414), 57–74.

Ernst, J. and Kellis, M. (2015). Large-scale imputation of epigenomic datasets for systematic annotation of diverse human tissues. *Nature Biotechnology*, **33**(4), 364–76.

Farlik, M., Sheffield, N. C., Nuzzo, A., Datlinger, P., Schönegger, A., Klughammer, J., and Bock, C. (2015). Single-Cell DNA Methylome Sequencing and Bioinformatic Inference of Epigenomic Cell-State Dynamics. *Cell Reports*, **10**(8), 1386–1397.

Ficz, G., Hore, T. A., Santos, F., Lee, H. J., Dean, W., Arand, J., Krueger, F., Oxley, D., Paul, Y. L., Walter, J., Cook, S. J., Andrews, S., Branco, M. R., and Reik, W. (2013). FGF signaling inhibition in ESCs drives rapid genome-wide demethylation to the epigenetic ground state of pluripotency. *Cell Stem Cell*, **13**(3), 351–359.

Gelfand, A. and Smith, A. F. M. (1990). Sampling-Based Approaches to Calculating Marginal Densities. *Journal Of The American Statistical Association*, **85**(410), 398–409.

Genereux, D. P., Johnson, W. C., Burden, A. F., Stöger, R., and Laird, C. D. (2008). Errors in the bisulfite conversion of DNA: modulating inappropriate-and failed-conversion frequencies. *Nucleic acids research*, **36**(22), e150.

Guo, H., Zhu, P., Wu, X., Li, X., Wen, L., and Tang, F. (2013). Single-cell methylome landscapes of mouse embryonic stem cells and early embryos analyzed using reduced representation bisulfite sequencing. *Genome Research*, pages 2126–2135.

Hou, Y., Guo, H., Cao, C., Li, X., Hu, B., Zhu, P., Wu, X., Wen, L., Tang, F., Huang, Y., and Peng, J. (2016). Single-cell triple omics sequencing reveals genetic, epigenetic, and transcriptomic heterogeneity in hepatocellular carcinomas. *Cell research*, **26**(3), 304–19.

Hubert, L. and Arabie, P. (1985). Comparing partitions. *Journal of Classification*, **2**(1), 193–218.

Jones, P. A. (2012). Functions of DNA methylation: islands, start sites, gene bodies and beyond. *Nature Reviews Genetics*, **13**(7), 484–92.

Kapourani, C. A. and Sanguinetti, G. (2016). Higher order methylation features for clustering and prediction in epigenomic studies. *Bioinformatics*, **32**(17), i405–i412.

Kapourani, C. A. and Sanguinetti, G. (2018). BPRMeth: a flexible Bioconductor package for modelling methylation profiles. *Bioinformatics*, **34**(14), 2485–2486.

Kelsey, G., Stegle, O., and Reik, W. (2017). Single-cell epigenomics: Recording the past and predicting the future. *Science*, **358**(6359), 69–75.

Krueger, F. and Andrews, S. R. (2011). Bismark: A flexible aligner and methylation caller for Bisulfite-Seq applications. *Bioinformatics*, **27**(11), 1571–1572.

Krueger, F., Kreck, B., Franke, A., and Andrews, S. R. (2012). DNA methylome analysis using short bisulfite sequencing data. *Nature Methods*, **9**(2), 145–151.

Luo, C., Keown, C. L., Kurihara, L., Zhou, J., He, Y., Li, J., Castanon, R., Lucero, J., Nery, J. R., Sandoval, J. P., Bui, B., Sejnowski, T. J., Harkins, T. T., Mukamel, E. A., Behrens, M. M., and Ecker, J. R. (2017). Single-cell methylomes identify neuronal subtypes and regulatory elements in mammalian cortex. *Science*, **357**(6351), 600–604.

Mayo, T. R., Schweikert, G., and Sanguinetti, G. (2015). M 3 D: A kernel-based test for spatially correlated changes in methylation profiles. *Bioinformatics*, **31**(6), 809–816.

McLachlan, G. and Peel, D. (2004). *Finite mixture models.* John Wiley & Sons.

Mulqueen, R. M., Pokholok, D., Norberg, S. J., Torkenczy, K. A., Fields, A. J., Sun, D., Sinnamon, J. R., Shendure, J., Trapnell, C., O'Roak, B. J., Xia, Z., Steemers, F. J., and Adey, A. C. (2018). Highly scalable generation of DNA methylation profiles in single cells. *Nature Biotechnology*, **36**(5), 428—-431.

Powers, D. (2011). Evaluation: From Precision, Recall and F-Measure to ROC, Informedness, Markedness & Correlation. *Journal of Machine Learning Technologies*, **2**(1), 37–63.

Schwartzman, O. and Tanay, A. (2015). Single-cell epigenomics: techniques and emerging applications. *Nature Reviews Genetics*, **16**(12), 716–726.

Shapiro, E., Biezuner, T., and Linnarsson, S. (2013). Single-cell sequencing-based technologies will revolutionize whole-organism science. *Nature Reviews Genetics*, **14**(9), 618–630.

Smallwood, S. a., Lee, H. J., Angermueller, C., Krueger, F., Saadeh, H., Peat, J., Andrews, S. R., Stegle, O., Reik, W., and Kelsey, G. (2014). Single-cell genome-wide bisulfite sequencing for assessing epigenetic heterogeneity. *Nature Methods*, **11**(8), 817–20.

Vanderkraats, N. D., Hiken, J. F., Decker, K. F., and Edwards, J. R. (2013). Discovering high-resolution patterns of differential DNA methylation that correlate with gene expression changes. *Nucleic Acids Research*, **41**(14), 6816–6827.

Zhang, W., Spector, T. D., Deloukas, P., Bell, J. T., and Engelhardt, B. E. (2015). Predicting genome-wide DNA methylation using methylation marks, genomic position, and DNA regulatory elements. *Genome biology*, **16**(1), 14.